Electron paramagnetic resonance, Optical absorption and Raman spectral studies on a pyrite/chalcopyrite mineral

G.Udayabhaskar Reddy[1], K.Seshamaheswaramma[1], Yoshinobu Nakamura[2], S. Lakshmi Reddy[1*], Ray L. Frost[• 3] and Tamio Endo[4]

1. Dept. of Physics, S.V.D.college, Kadapa 516 003, India
2. Dept. of Applied chemistry, School of Engineering, The University of Tokyo, Japan.
3. Inorganic Materials Research Program, Qeensland University of Technology
   2 George Street, Brisbane, GPO Box 2434, Queensland 4001, Australia.
4. Faculty of Engineering, Mie University, TSU, Mie 514 8507, Japan

Abstract

A pyrite/chalcopyrite mineral sample from Mangampet barite mine, Kadapa, Andhra Pradesh, India is used in the present study. XRD data indicates that the pyrite mineral is face centered cubic lattice structure with lattice constant 5.4179 A.U. Also it possesses an average particle size of 91.6 nm. An EPR study on the powdered pyrite sample confirms the presence of iron whereas in chalcopyrite both iron and Mn(II) are present. The optical absorption spectrum of chalcopyrite is due to copper, which is in a distorted octahedral environment. NIR results confirm the presence of water fundamentals. Whereas the Raman spectrum is due to water and sulphate ions.

Key words: Pyrite/chalcopyrite, XRD, EPR, optical absorption spectra, NIR spectra, Raman spectrum, Fe(II), Cu(II), Mn(II)

• Author to whom correspondence should be addressed (r.frost@qut.edu.au)
T: +61 7 3138 2407 F: +61 7 3138 1804
Queensland University of Technology, Faculty of Science and Technology, 2 George St., Brisbane, Queensland Australia 4001
*Corresponding author email:drslreddy_in@yahoo.com

Introduction

Minerals of geological interest are structurally and chemically complex compared with most inorganic solids. Because of this complexity, many spectroscopic methods have been utilised to answer fundamental questions about their state or order, energetics and structure property relationships. Structural methods that are element specific and give localised structural information. These methods include Mossbauer, optical absorption, XPS, NMR and EPR spectroscopic studies.

The pyrite group of minerals has the general formula AX_2, where A can be Fe, Zn, Hg, Au, Co, Cu, Mn, Ni, Ir, Pd, Pt or Ru and X can be S, As, Sb, Bi, Se and Te. Among them pyrite is the common mineral. Pyrite is also called "Fools Gold" because of its similarity in color, shape and habit to gold. It is lighter than gold. Pyrite is most valuable in the production of sulphuric acid. Pyrite is an iron sulphide with the formula FeS_2. It is a semiconductor with band gap of 0.95 ev [1]. Pyrite readily changes by oxidation to an iron sulfate or to the hydrated oxide. The unit cell is composed of an iron face centered cubic sub lattice into which sulphur ions are embedded. Pyrite structure is similar to fluorite and NaCl in which the positions of chlorine atoms occupy twinned dumbbell pair anions with cell edge constant a = 5.42 AU. Molecular sulphide ion (S_2^{2-}) oriented along the axis of third order, while Fe^{2+} ions are into the centre of the octahedral [2]. Each iron atom is surrounded by six sulfur atoms at the corners of the octahedral [3]. Measurements of X-ray absorption edges on chalcopyrite suggest that copper is present in two valence states, so that resonance between Cu^{+}+Fe^{3+} and Cu^{2+} + Fe^{2+} may be presumed [4].

Mössbauer spectra of naturally occurring mineral chalcopyrite have been undertaken over a temperature range 300°–448°K [5]. Mössbauer studies on natural Egyptian chalcopyrite have been reported and reveal that most of the iron is in Fe^{+2} state and to a lesser extent in Fe^{+3} state [6]. X ray diffraction (XRD) on natural and synthetic pyrite minerals were reported [7.]. Absorption Spectra of $CuFeS_2$ and Fe-Doped $CuAlS_2$ and $CuGaS_2$ have been studied [8]. The chemical analysis of chalcopyrite originated from

Karnataka, India is reported and reveal that it contains Cu = 25.00, Fe = 27.90, S= 26.92 and Pb or Zn = 0.75 Wt% [9]

To date no Mössbauer, optical absorption, electron paramagnetic resonance (EPR) and Raman spectral studies have been carried out on pyrite/chalcopyrite mineral originating from the baryte mine of Magampet, Kodur, Kadapa district, India. In this study we report XRD, EPR, optical absorption Raman and Mössbauer spectral studies and relate these studies to the structure of the mineral.

Experimental

A brownish yellow coloured pyrite/chalcopyrite mineral originated from baryte mine Mangampet, India is used in the present work. It is evident from the chemical analysis that the mineral pyrite contains 56.8 wt% of iron and chalcopyrite contain 26.8 wt% of iron and 28.2 wt% of copper.

X-ray powder diffraction pattern of pyrite is recorded in Philips X-ray diffractometer operated in reflection geometry at 30 mA, 40 kV with Cu-K_α (λ = 1.54060 AU) source at 25 ºC from 10º-75º. Data was collected using a continuous scan rate of 1º /2 min^{-1} which was then refined into $^{\circ}$2 theta steps of 0.02°.

EPR spectra of pyrite and chalcopyrite powdered samples are recorded both at room (RT) and liquid nitrogen temperature (LNT) on JEOL JES TE100 ESR spectrometer operating at X band frequency (υ =9.40531GHz for pyrite and 9.40620 GHz for chalcopyrite) having a 100 KHz field modulation to obtain first derivative EPR spectrum. DPPH with a g value of 2.0036 is used for a g factor calucation.

Optical absorption spectrum of the chalcopyrite sample is recorded at room temperature on Carey 5E UV-Vis-NIR spectrophotometer in mull form in the range 200-2000 nm.

The chalcopyrite powdered mineral sample was placed and oriented on the stage of an Olympus BHSM microscope, equipped with 10x and 50x objectives and part of a Renishaw 1000 Raman microscope system. Raman spectra were excited by He-Ne laser

(633nm) at a resolution of 2 cm^{-1} in the range between 100 and 4000 cm^{-1}. Other details of the experimental technique have already been reported [8, 9]

Band component analysis was undertaken using the Jandel "PEAKFIT" software package which enabled the type of fitting function to be selected and specific parameters to be fixed or varied accordingly. Band fitting was carried out using a Lorentz–Gauss cross product function with a minimum number of component bands used for the fitting process (cross product function is a mathematical function). The Lorentz–Gauss ratio was maintained at values greater than 0.7 and fitting was undertaken until reproducible results were obtained with squared correlations of r^2 greater than 0.9975.

Theory

Various EPR parameters such as g, A, D and E are employed while interpreting EPR spectrum. The *g* parameter is a measure of the coupling between the unpaired electron's spin angular momentum (*S*) with its orbital angular momentum (*L*) [10]. The unpaired electron interacts (couples) with the nuclear spin (*I*) to form a $(2I + 1)$ line hyperfine structure centered on *g* and spaced with the distance quantified by the hyperfine coupling parameter *A*. The coupling between the nuclear and electron spins becomes stronger as the *A* parameter becomes larger. The combination of *g* and *A* parameters can be utilized to differentiate between electron environments of Fe^{3+} and Mn^{2+} ions. The EPR zero field splitting (ZFS) parameters, *D* and *E,* measure the deviation of the ion crystal field from ideal tetrahedral or octahedral symmetries and they apply to ions with more than one unpaired electron, e.g., low field Fe^{3+} and Mn^{2+}. However, the broad nature of EPR spectra of Fe^{3+} makes the determination of *D* and *E* difficult [11].

Mn(II), being a d^5 ion, has total spin S = 5/2. The state splits into three Kramers' doublets, $\pm 5/2\rangle$, $\pm 3/2\rangle$and $\pm 1/2\rangle$ separated by 4D and 2D respectively, where D is the zero-field splitting parameter. The deviation from axial symmetry leads to a term known as E in the spin Hamiltonian. The parameter of E can be easily calculated from single crystal measurements. A non-zero value of E results in making the spectrum unsymmetrical about the central sextet.

Cu(II) has an electronic configuration [Ar] $3d^9$. In an octahedral crystal field, the corresponding ground state electronic configuration is $t_{2g}^6 e_g^3$ which yields ^2E_g term. The excited electronic configuration $t_{2g}^5 e_g^4$ corresponds to $^2T_{2g}$ term. Hence, single electron transition $^2E_g \rightarrow {}^2T_{2g}$ is expected in an octahedral crystal field. Normally, the ground ^2E_g state splits due to Jahn-Teller effect and hence lowering of symmetry is expected for Cu(II) ion. This state splits into $^2B_{1g}(d_x^2\text{-}_y^2)$ and $^2A_{1g}(d_z^2)$ states in tetragonal symmetry and the excited term $^2T_{2g}$ also splits into $^2B_{2g}(d_{xy})$ and $^2E_g(d_{xz},d_{yz})$ levels. In rhombic field, ^2E_g ground state splits into $^2A_{1g}(d_x^2\text{-}_y^2)$ and $^2A_{2g}(d_z^2)$ whereas $^2T_{2g}$ splits into $^2B_{1g}(d_{xy})$, $^2B_{2g}(d_{xz})$ and $^2B_{3g}(d_{yz})$ states. Thus, three bands are expected for tetragonal (C_{4v}) symmetry and four bands are expected for rhombic (D_{2h}) symmetry [12].

The ground state configuration of Fe(II) ion is $3d^6$. In an octahedral field, assuming high spin state, the configuration is expressed as $t_{2g}^4 e_g^2$. This configuration gives rise to electronic states $^5T_{2g}$, ^3E_g, $^3T_{2g}$ and some more triplets and singlets of which $^5T_{2g}$ forms the ground state. The other excited configurations, such as $t_{2g}^3 e_g^3$ gives rise to a several triplet and singlet states and one quintet state designated as ^5E_g. Thus the spin allowed transition $^5T_{2g} \rightarrow {}^5E_g$ is expected to be strong and all other spin forbidden transitions are very weak [13, 14]. Thus, the $^5T_{2g} \rightarrow {}^5E_g$ transition gives an intense, but broad absorption band. Often this band splits into two in an octahedral environment. If the splitting is of the order of 2000 cm^{-1}, then it is due to static distortion of octahedron [15 -17]. However, an intermediate value between 100 and 2000 cm^{-1} indicates a dynamic Jahn-Teller effect in the excited ^5E_g state [18, 19]. In the latter case, the energy level split symmetrically to the center of gravity and the average of these values of these bands is to be taken as 10Dq value.

Results and Discussion

X-ray diffraction results

Fig. 1 shows the diffraction pattern of pyrite mineral recorded on Philips diffractometer at 25ºC. The peak is characterized by using Scherrer formula. The

143 powder difraction pattern is similar to that of the spectra reported for pyrite [20]. The
144 peak list of pyrite sample is presented in Table 1.

145

146 **Table 1**

147 **XRD peak list data of pyrite mineral**

S.No	Positions [º2Th]	Miller Indices			Height (cts)	FWHM [º2Th]	d-spacing [$\overset{0}{A}$]	Relative intensity [%]	Unit cell constant $\overset{0}{A}$	Particle density (grain size) $\overset{0}{A}$
		h	K	L						
1	28.512	1	1	1	10.28	0.2880	3.12803	38.3	5.4179	**4.97**
2	33.040	2	0	0	56.83	0.0720	2.70895	100	5.4179	**20.09**
3	37.074	2	1	0	32.34	0.1920	2.42296	67.7	5.4179	**7.22**
4	40.762	2	1	1	27.66	0.1920	2.21185	54.9	5.4179	**7.70**
5	47.424	2	2	0	23.26	0.1920	1.91552	49.0	5.4179	**7.89**
6	50.495	2	2	1			1.80597	0.6	5.4179	
7	56.270	3	1	1	94.83	0.1200	1.63356	98.4	5.4179	**13.10**
8	59.012	2	2	2	20.21	0.2400	1.56401	14.6	5.4179	**6.64**
9	61.678	0	2	3			1.50266	17.1	5.4179	
10	64.279	3	2	1	12.74	0.2880	1.44799	23.1	5.4179	**5.68**
11	69.320	4	0	0			1.35448	0.4	5.4179	

12	71.777	4	1	0			1.31403	0.6	5.4179	
13	74.200	4	1	1			1.27701	0.3	5.4179	

This calculated unit cell value well agreed with reported value on pyrite sample [21]. This conforms that the sample is pyrite to cubic octahedral structure. The X-ray density 'd_x' is calculated using the formula [22] $d_x = \frac{ZM}{Na^3}$

Here "*Z*"(4) represents the number of molecules in a unit cell of the pyrite lattice 'M' (119.98 gm) is the molecular weight of the mineral, 'N' is the Avogadro's number and 'a' the lattice constant of the sample. The calculated value of X-ray density is 5.01195 g/cm^3. The percentage porosity of each sample was calculated using the relation [23]

Percentage porosity (p%) = $\left[1 - \frac{d}{d_x}\right]100$.

Here, 'd' is bulk density (pyrite = 4.84 g/cm^3).

The calculated value of porosity percentage is 3.43. The grain size of the compound is evaluated from the line broadening of the peaks using Debye-Scherrer equation

$$D_{(hkl)} = \frac{0.9\lambda}{\beta_{1/2}\cos\theta}$$

Here D is the average particle size of the crystal

λ is the wavelength of incident X ray

θ is the corresponding Bragg angle

$\beta_{1/2}$ is the full width at half maximum (FWHM) of the peak. The average particle size of the crystal is calculated as 91.6 nm. The crystal is face centered cube.

EPR Results

The pyrite/chalcopyrite mineral originated from Mangampet, Kadapa, India, is brownish yellow in colour is used in the present work. The EPR spectrum of the pyrite mineral sample recorded at room temperature is shown in Fig. 2. Even at low temperature the structure could not be observed. Probably this might be due to the very high

concentration of iron present in the mineral. However, only a single peak with g= 2.38 could be observed in the spectrum at room temperature.

Fig. 3 shows the EPR spectrum of chalcopyrite mineral recorded at room temperature in the range 0-500 mT. It shows various resonances with g values of 3.77, 3.19, 2.46, 2.46, 2.18 and a sextet hyperfine structure of with g value of 1.998. The expanded version of the sextant of the sample is shown in Fig.4. The spectrum consists of a high intense sextet with g=1.998 and A =7.90 mT. This indicates that more Mn (II) ions are present in the octahedral environment. Further the presence of resolved hyperfine structure at g =1.998 resonance strongly indicates that Mn(II) ions in symmetric sites (octahedral) are isolated or significantly distant from each other The strong resonance line in lower field with g = 3.19 and other weak resonances with g values 3.77, 2.46 and 2.18 are also due Mn(II) in distorted octahedral crystalline field in the chalcopyrite mineral. The lack of hyperfine splitting at g = 3.19, 3.77 resonance lines are due to fluctuations of the ligand field parameters in the Mn(II) ion neighborhood and random distributions of the structural distortions[24].

The hyperfine constant 'A' value provides a qualitative measure of the ionic nature of bonding with Mn(II) ion. The percentage of covalency of Mn-ligand bond has been calculated using 'A' (8.0 mT) value obtained from the EPR spectrum and Matumura's plot [25]. It corresponds to an ionicity of %. Also the approximate value of hyperfine constant (A) is calculated by using covalency (C) equations [26,27]

$$A_{iso} = (2.04C - 104.5)\ 10^{-4}\ cm^{-1}.$$

The value obtained is 91x 10^{-4} cm^{-1}. This calculated value agrees well with the observed hyperfine constant for the sample indicating ionic character for Mn-O bond in the mineral under study. The number of ligands around Mn(II) ion is estimated using the covalency [28] equation for C

$$C = \frac{1}{n}\left[1 - 0.16\left(X_p - X_q\right) - 0.035\left(X_p - X_q\right)^2\right]$$

Here X_P and X_q represent electro-nagativities of metal and ligand. Assuming $X_p = X_{Mn} =$ 1.6 and $X_q = X_S = 3.5$, the number of ligands (n) obtained are 16. This suggests that Mn(II) may be surrounded by four SO_4^- . Further, the g value for the hyperfine splitting is indicative of the nature of bonding. If the g value shows negative shift with respect to free electron g value of 2.0023, the bonding is ionic and conversely, if the shift is positive, the bonding is more covalent in nature [29]. In the present work, from the observed negative value of $4.3x10^{-3}$, it is apparent that the Mn(II) is in an ionic environment. Depending on the charge considerations, the impurity might have entered the lattice in place of Zn(II).

In the high spin ground states ^6S, Fe^{2+} ions under go no first order spin orbit interactions and 'g ' is expected to be near the free electron value is 2 since experimental data reveals that values much higher than 2 , the theory of large g values based on the spin Hamiltonian [30] was used for the interaction of the EPR spectrum.

$\hat{H} = g\beta SB + D(S_z^2 - S(S+1)/3) + E(S^2_x - S^2_y)$

Here β – Bohr magneton , S – the effective spin , g a second rank tensor with Eigen values g_x, g_y, g_z. $D(=3B_Z^0)$ is the axial and $E(= B^2_Z)$ the orthorhombic component which describes the splitting of the Fe(III) Kramers doublets in crystal field . The orthorhombic electrons of the field is E/D=λ. For completely rhombic field λ= E/D=0.33 and for axial symmetry E/D=0 . A single EPR signal with $g_{x=} g_y= g_z = 4.27 = g_{eff}$ will be observed when λ=0.33 and hν/D < 1 (hν microwave energy) [31]

According to this calculation the g_{eff} values of 3.77 and 3.19 corresponds to Fe^{3+} centers with λ =0.27 this means that the crystal field at the Fe^{3+} centers in chalcopyrite is of strong orthorhombic character . The structure of the EPR lines at 3.77 and 3.19 suggest that Fe(III) is in two structurally in equivalent centers in chalcopyrite .

Optical absorption spectral analysis

Optical absorption spectrum of chalcopyrite mineral recorded in mull form from 200 to 800 nm and its peak fit analysis is shown in Fig. 5. It consists of bands at 16025, 27320, 35715, 36765, 44445 and 48310 cm^{-1}. Where as NIR spectrum recorded from 800- 1500 nm and its peak fit analysis is shown in Fig. 6. It shows energies at 10780, 8400, 8245, 7215, 6955, 6755 and 5017 cm^{-1}. Ferrous and ferric ion complexes derive strong bands in NIR spectrum. The bands at 8400, 10780, 16025 and 27320 cm^{-1} in the UV-Vis, NIR regions are assigned to Cu(II) in rhombic symmetry. The general ordering of the energy levels for rhombic symmetry is as follows [32] $A_{1g}(d_x^2\text{-}_y^2) < {}^2A_{2g}(d_z^2) < {}^2B_{1g}(d_{xy}) < {}^2B_{2g}(d_{xz}) < {}^2B_{3g}(d_{yz})$. Accordingly, the optical absorption bands observed of chalcopyrite min mineral are 8400, 10780, 16025 and 27320 cm^{-1} [Table-2]. These energies are comparable with the other data reported for copper containing samples [33-37]. The appearance of two sharp bands at 8245 cm^{-1} and 10780 cm^{-1} indicates ferrous ion in the chalcopyrite mineral. The average of these bands 9513 cm^{-1} is taken as 10 Dq band for Fe(II) ion and is assigned to ${}^5T_{2g} \rightarrow {}^5E_g(D)$. Accordingly the Dq value is different 951 cm^{-1}. The splitting of 10Dq band (10780 – 8245 = 2535 cm^{-1}) indicates that it is due to Jahn-Teller effect in the excited ${}^5E_g$ state.

The bands observed at 35715, 36765, 44445 and 48310 cm^{-1} might be a charge transfer bands. The energies observed at 7215, 6955, 6760 cm^{-1} are not d-d transitions. The OH^- stretching mode gives rise to the most common features in near infrared region. Hydroxyl exists as part of the structure and the stretching mode appears whenever water is present in any form [the range 3645 to 3677 cm^{-1}]. The ν_{OH} overtone ($2\nu_{OH}$) gives rise to a band in the NIR spectrum [38]. Accordingly the band observed at 7413 cm^{-1} (3706 x $2 = 2\nu_{OH}$) is assigned to the first overtone of OH. The band at 5017 cm^{-1} is the combination of the frequency lattice modes [39].

Table – 2

Comparison of energies of the bands with their assignments for Cu(II) in rhombic octahedral coordination with ground state $^2A_{1g}(d_x2_{-y}2)$

Sample	$^2A_{1g}(d_Z^2)$		$^2B_{1g}(d_{XY})$		$^2B_{2g}(d_{XZ})$		$^2B_{3g}(d_{YZ})$		Reference
	cm^{-1}	nm	cm^{-1}	Nm	cm^{-1}	Nm	cm^{-1}	Nm	
Antlerite $Cu_3SO_4(OH)_4$	8475	1180	9435	1060	10990	910	16390	610	[33]
Turquoise $CuAl_6(PO_4)(OH)_84H_2O$			14970	668			18354	545	[34]
ZPPH $(ZnKPO_4)6H_2O$	7750	1290	9613	1040	12117	825	13330	750	[35]
Atacamite $Cu_2(OH)_3Cl$	8049	1242	10296	971	11083	902	15380	650	[36]
Libethenite Cu_2PO_4OH	8920	1121	11820	846	14925	670	20450	489	[37]
Chalcopyrite $(Cu,Fe)S_2$	8400	1190	10780	928	16025	624	27320	366	Present work

Fig. 5 clearly indicates Charge transfer energies at 35715, 36765, 44445 and 48310 cm^{-1}. These bands are assigned to charge transfer transitions to metal ligand.

NIR Results

The NIR spectrum shown in Fig. 6 consists of group of three sharp and strong bands located at 7215, 6955 and 6755 cm^{-1} are due to molecular water. Water in fluid inclusions in the chalcopyrite is probably the cause these bands

Raman spectral analysis

Raman spectrum of chalcopyrite mineral recorded at RT in the range 100 to 600 cm^{-1} is shown in Fig. 7 and in the range 600 to 1700 shown in Fig. 8. A low intensity sharp Raman band observed at 430 cm^{-1} is assigned to $\nu_2(A_g)SO_4$. Very sharp high intensity bands observed at 345, 385 cm^{-1} are due to sulphate bending modes. A broad and weak band observed at 150 cm^{-1} is probably due to hydrogen bonding. An independent sharp band observed at 1020 cm^{-1} is due to $\nu_1(A_g)SO_4$. Highest intensity band observed with weak shoulders on either side is observed at 1330 cm^{-1} is due to $\nu_3(E)SO_4$. A couple of bands observed at 1495 and 1620 cm^{-1} overlapped by one another are attributed to OH stretch $\nu_2(H_2O)$

Conclusions

1. XRD data indicating that pyrite [FeS_2], is a iron sulphide with cubic cell constant A = 5.419 A.U. with average particle grain size of 9. 19 A.U.

2. The EPR studies on pyrite confirming the presence of iron which is in very high concentration. Whereas in chalcopyrite along with iron and copper manganese is also present in traces.

3. Optical absorption spectrum of chalcopyrite is due to Fe(II)/Cu(II) which is in distorted octahedral symmetry.

4. Mid-infrared spectral studies are indicative of combination over tones and combination tones of water fundamentals and sulphate

5. Raman spectrum of chalcopyrite mineral is due to sulphate and water molecules.

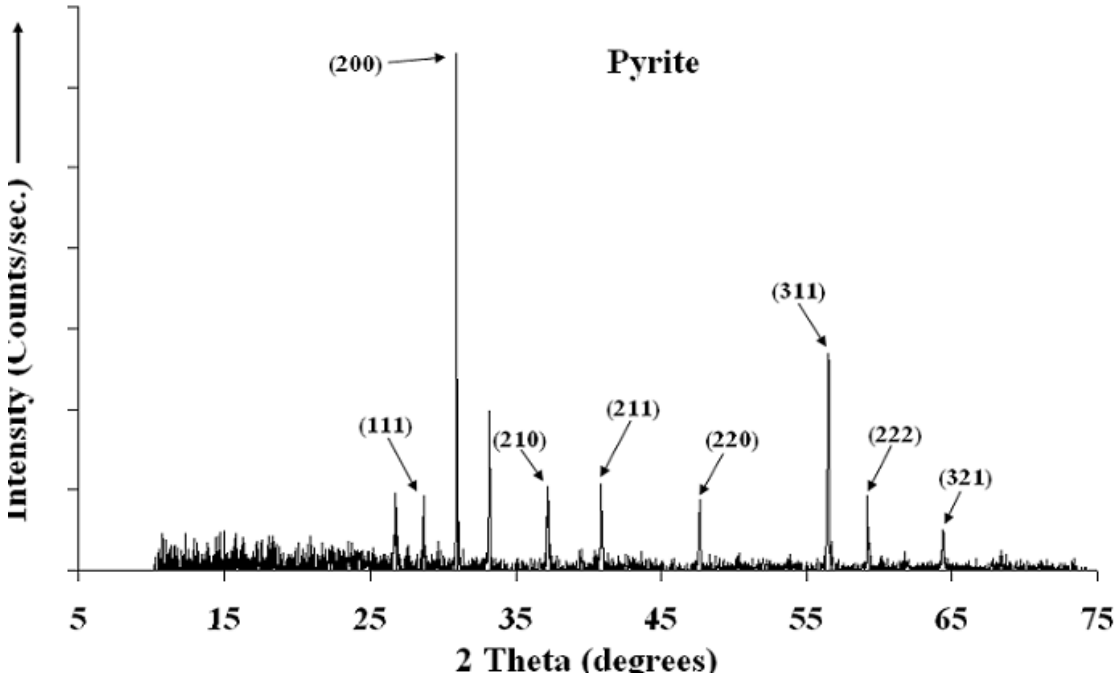

294
295 Fig.1 Powder X ray diffraction pattern [Cu K_α] for pyrite mineral at 25ºC

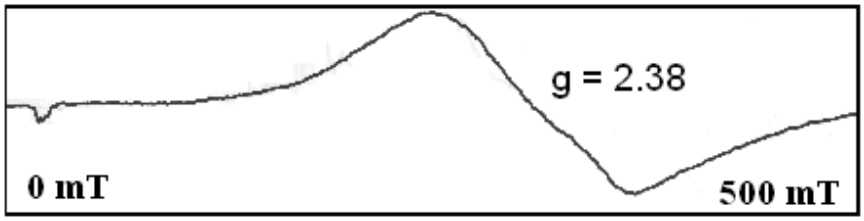

296

297 Fig.2 EPR spectrum of pyrite mineral at RT (ν = 9.40531 GHz)

298

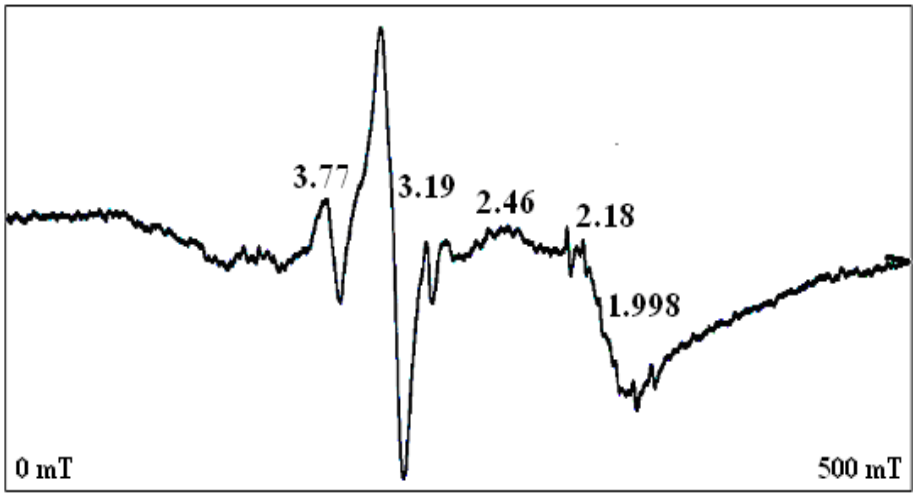

Fig.3 Powdered EPR spectrum of chalcopyrite mineral at RT (υ =9.40619)

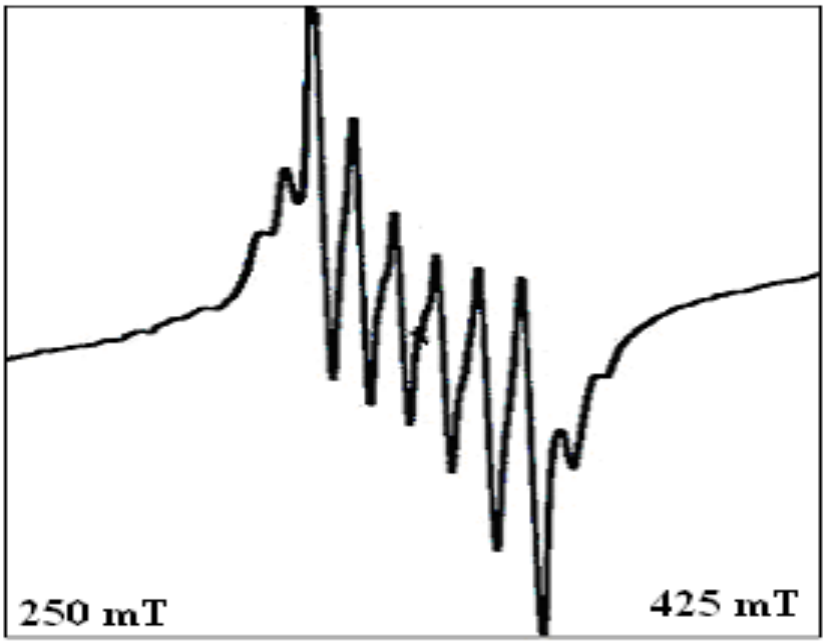

Fig. 4 Expanded version of chalcopyrite mineral at RT (υ =9.40620)

307

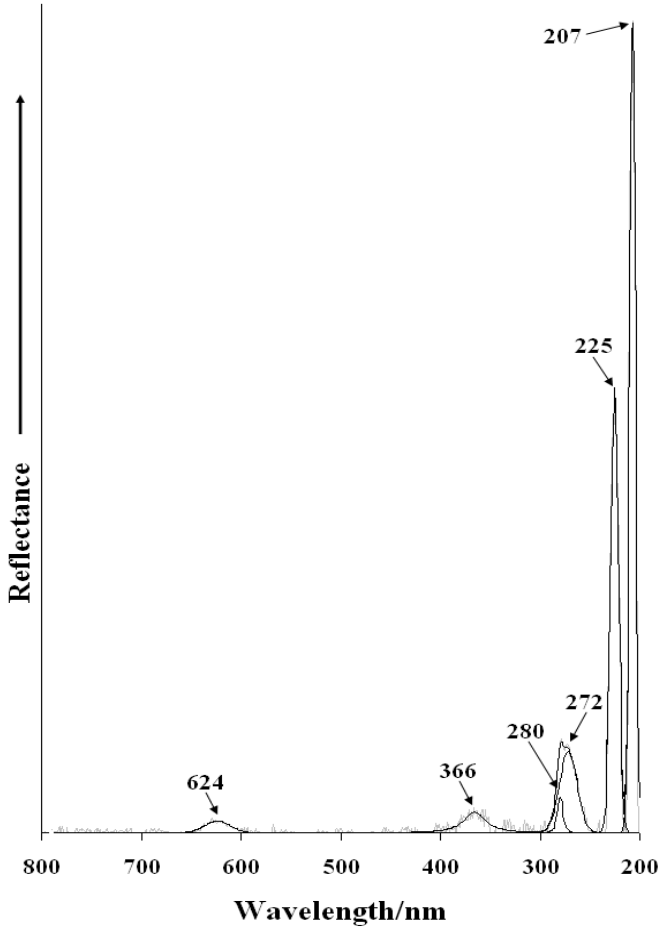

308

309 Fig. 5. Optical absorption spectrum of chalcopyrite at room temperature

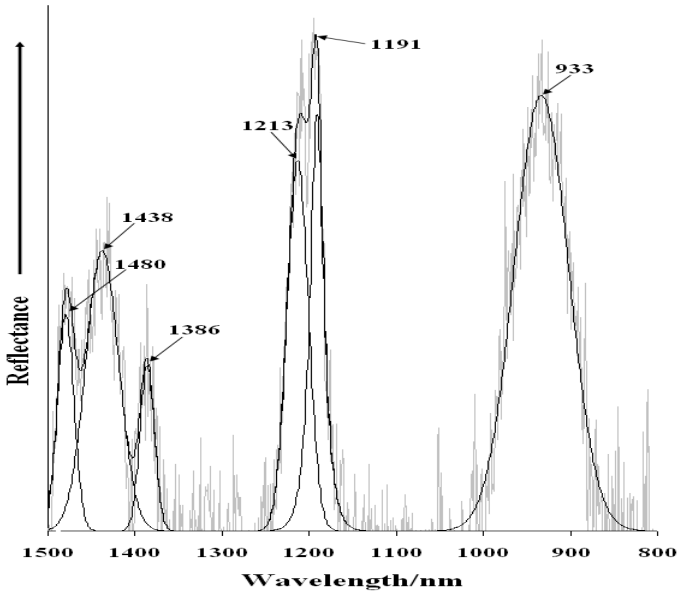

310

311 Fig. 6 NIR spectrum of chalcopyrite mineral at room temperature

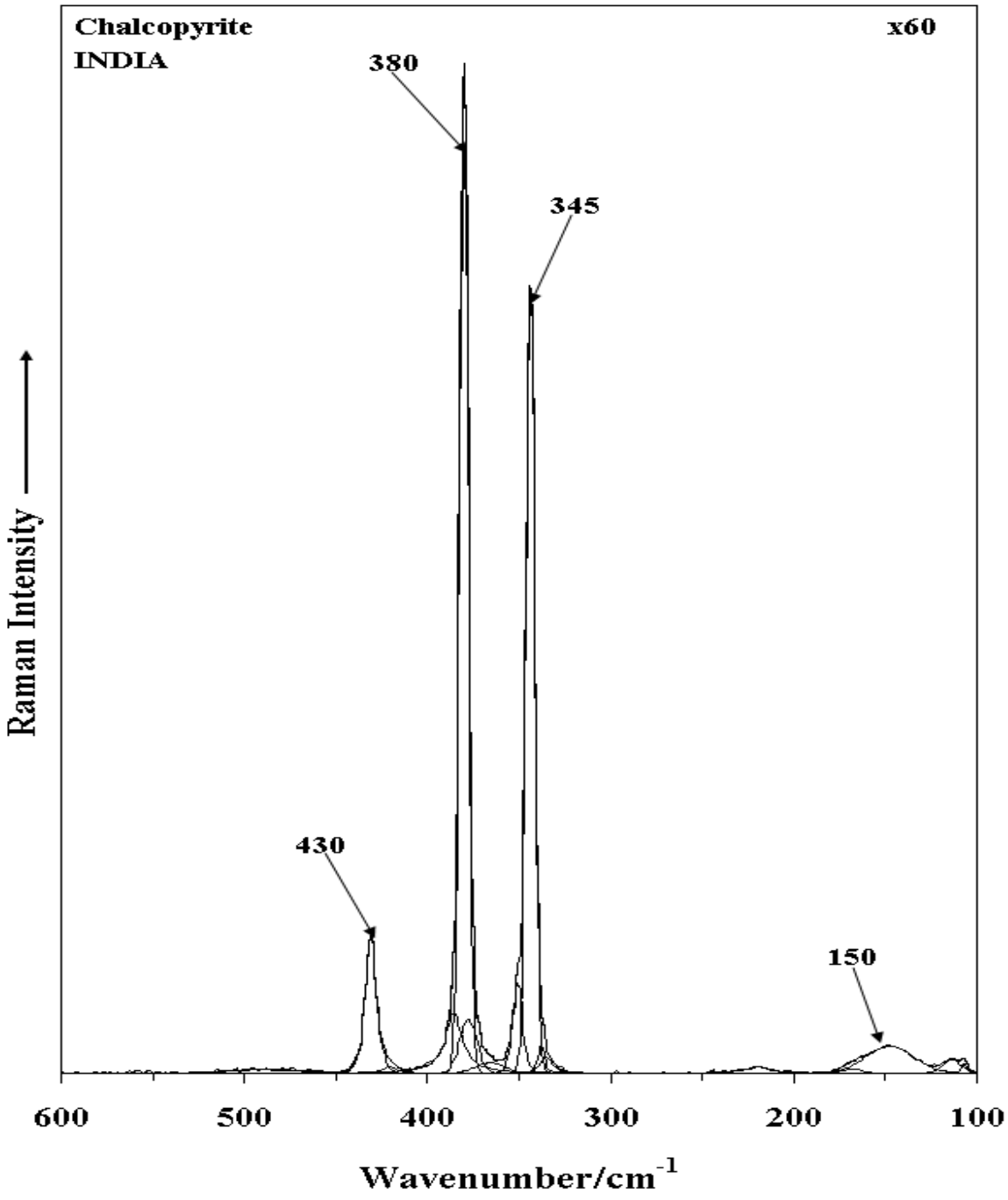

312

313 **Fig. 7 Raman spectrum of chalcopyrite mineral at room temperature in the range**

314 **100 – 600 cm^{-1}**

315

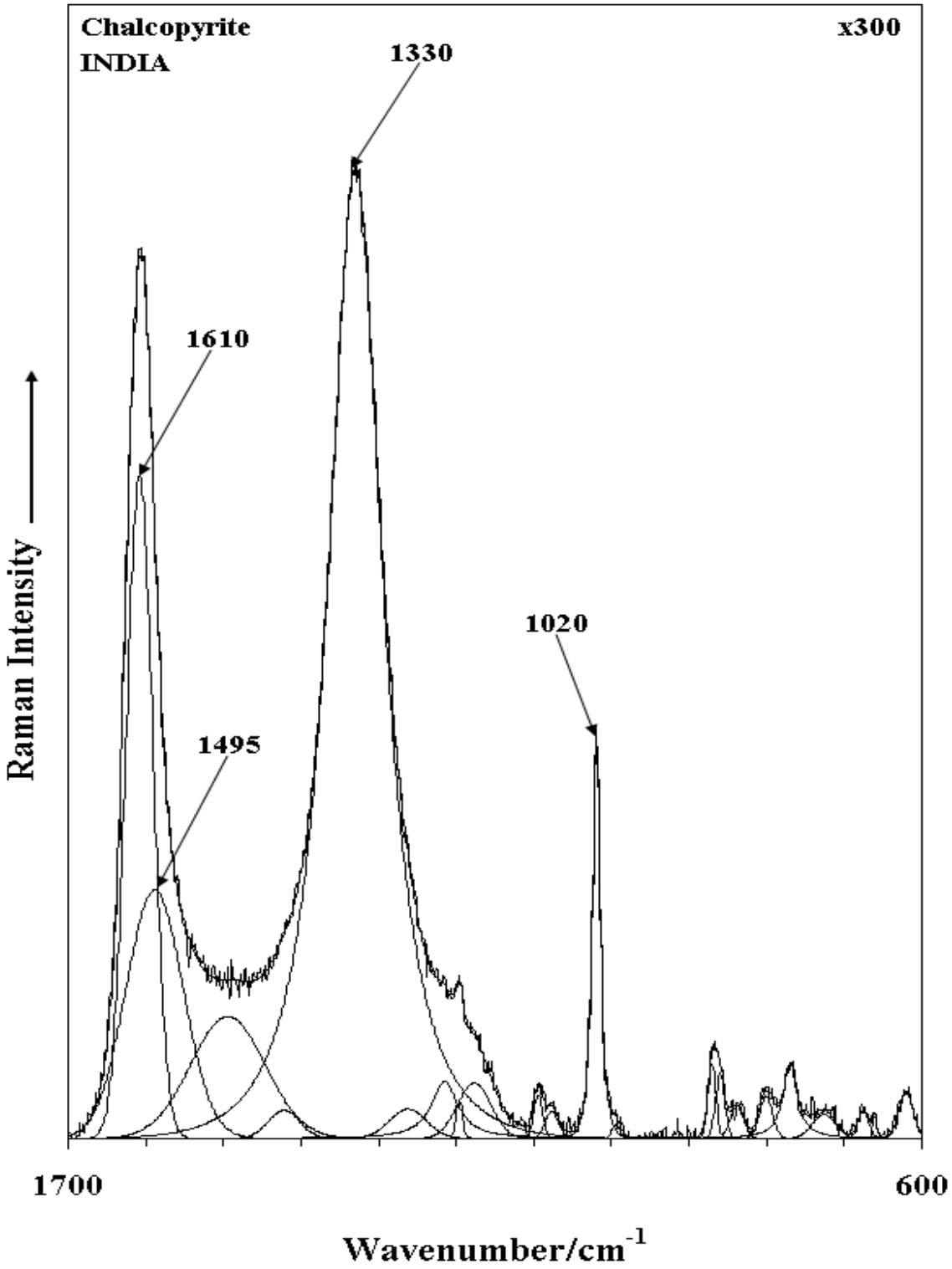
Chalcopyrite
INDIA
x300
1330
1610
1020
1495
Raman Intensity
1700
600
Wavenumber/cm-1

316

Fig. 8 Raman spectrum of chalcopyrite mineral at room temperature in the range 600 – 1700 cm^{-1}

References

1. K. Ellemer and H. Tributch Proceedings of the 12th Workshop on Quantum Solar energy Conversion (2000)
2. A. V. Milovsky and O.V Kanonov, “Minerology”, Mir publishers (1985) pp.121
3. W. A. Deer, R. A. Howie and J.Zussman, ELBS Edition (1978) pp.445, London
4. C. Kurylenkxo, Bull. Soc. Franc. Min. Crist. 65 (1942) 45.
5. Deo Raj, K. Chandra and S. P. Puri , J. Phys. Soc. Jpn. 24 (1968) 39-41.
6. N. A. Eissa, H. A. Sallam, M. M. El-Ockr, E. A. Mahoud and S. A. Saleh, J. Physics Colloque C6, supplement article No: 12, 37 (1976) C6-793.
7. S. S. Udubasa, S. Constantinescu, M. N. Grecu, N. Popescu-Pgrion, Gh. Udubasa, Gh. C. Popescu, F. Tolea, I. V. Popescu, Rom. Journ. Phys., 52 (2007) 93–104 .
8. Teruo Teranishi, Katsuaki Sato and Ken'ichi Kondo, J. Phys. Soc. Japan. 36 (1974) 1618-1624.
9. M. Annesuddin, P. N. Char, M. Raza Hussain and E. R. Saxena, J.Therm. Anal. 26 (1983) 205-216.
10. M. Symons, “Chemical & Biological Aspects of Electron Spin Resonance Spectroscopy”, John Wiley & Sons, New York (1978.).
11. De Vos, B. M. Weckhuysen, and T. Bein., J. Am. Chem. Soc. 118 (1996) 9615.
12. M. A. Hitachmann and T. D. Waite, Inorg.Chem.,15, 2150 (1976).
13. G. H. Faye, Can. Min. 9,403 (1968).
14. C. J. Ballhausen, “Introduction to Ligand Field Theory”,Mc-Graw Hill Book Company, New Delhi (1962)
15. F.A. Cotton, M. Megers, J. Am. Chem. Soc., 82, (1960) 5023.
16. O. G. Holmes, D.S. McClure, J.Chem. Phys. 26 (1957) 1686
17. G. D. Jones, Phys. Rev. 155 (1967) 259.
18. G. H. Faye, Can. J. Earth Sci. 5 (1968) 3.
19. W. Low, M. Weger, Phys. Rev. B 118 (1960) 1130
20. J. F. Rilley, Amer. Miner, 53 (1968) 293-295.
21. S. S. Udubase et all structural investigation on some sulphides from costesti, valea lul stan and jidoctita gold ores 101.

22. V. Cerny, B. Petrova and M. Frumar, "Elements of X-ray Diffraction, Addition Wesley Reading", M A, 1959.
23. International Tables for X-ray Crystallography (Kynoch Press, Birmingham), Vol. III,210 (1968).
24. V. Carney, B. Petraova and M. Frumat, J.Non-Cryst. Solids 125 (1990) 17
25. O. Matumura, J. Phys. Soc. Japan, 14 (1959) 108.
26. E. Simanck, K. A. Muller, J. Phys. Chem. Solids 31 (1970) 1027.
27. A. M. F. Benial, V. Ramakrishnan, R. Murugesan, Spectrohimica Acta A 55 (1999) 2573
28. E. Simanck, K. A. Muller, J. Phys. Chem. Solids 31 (1970) 1027
29. V. Wieringen, Discuss. Faraday Soc. 19 (1955) 118
30. C. M. Brodbeck Non-crystalline solids 40 (1980) 305-313.
31. J. M. Gaite and J. Michoulier, J. Miner. Cryst., 93 (1970) 341-356.
32. M. A. Hitachmann and T. D.Waite, Inorg.Chem.,15, 2150 (1976).
33. R. Ramasubba Reddy, S. Lakshmi Reddy, G. Siva Reddy, B. J. Reddy, Cryst. Res. Tech. 37,485(2002).
34. K. B. N. Sharma, L. R. Murthy, B. J. Reddy and S.Vedanand, Phys. LettA.132, 293(1988).
35. N.Madhu, A.V.chandra Sekhar, B.J.Reddy, Y.P.Reddy & RVSSN Ravikumar, Indian J.Chem. 38A, 590(1999).
36. S. Lakshmi Reddy, K. Ramesh and B. J. Reddy, 3rd Asia Pacific Physics Conference, 20-24 June (1988) 994.
37. N. C. Gangi Reddy, R. Ramasubba Reddy, G. Siva Reddy , S. Lakshmi Reddy and B. Jagannatha Reddy EPR, Optical absorption, MIR and Raman Spectral studies on Libethenite mineral, Cryst.Reser.Tech. 41, 400-404 (2006)
38. G. R. Hunt, J.W. Salisbury, Mod. Geol., 1(1970.) 283
39. G. R. Hunt, J.W. Salisbury and C. Lenhoff, Mod. Geol., 3 (1971)1